

Tunable Terahertz Plasmon-Induced Transparency in Resonator-Coupled Dirac Semimetal Waveguides

Daobin Wang, Jiahuan Yang, Wei Wang, Lihua Yuan, and Xiaoxiao Li

Department of Applied Physics
Lanzhou University of Technology, Lanzhou, 730050, China
photonics_wang@yahoo.com

Abstract — The bulk Dirac semimetal (BDS) is an interesting material, similar to graphene, which can dynamically adjust its optical properties via a variation in its Fermi energy or electrical voltage. In this work, a BDS-based plasmonic device, which enables tunable terahertz plasmon-induced transparency, was proposed and designed. By using the finite element method, the surface plasmon polariton and plasmon-induced transparency of this device were systematically investigated. The results demonstrate that the plasmon-induced transparency of such device can be dynamically tuned by varying its Fermi energy. When the Fermi energy changes from 55 meV to 95 meV, the maximum group delay time of the device increases from 13.2 ps to 21 ps. In the case of a cascading device, the maximum group delay time can be further pushed up to 44.57 ps. The influence of the ambient refractive index on the optical properties of the proposed device was also considered and investigated.

Index Terms — Bulk Dirac semimetal, plasmon-induced transparency, surface plasmon polariton, slow light.

I. INTRODUCTION

Plasmon-induced transparency (PIT) is a novel physical phenomenon, which occurs at the interface between a metal and a dielectric material [1]. This phenomenon was first discovered in several atomic media, and it is known as electromagnetically induced transparency (EIT) [2, 3]. Later, it was found that a similar phenomenon can also be observed in photonic crystals [4], metamaterials [5], acoustic devices [6], coupled dielectric resonators [7], and nanodevices based on the surface plasmon polariton (SPP) [8]. The EIT effect that occurs at the interface between a metal and a dielectric material is known as PIT. The mechanism behind the PIT phenomenon and its application in various fields have triggered a strong interest in the scientific community around the world [9, 10].

Precious metals, such as gold, silver, and copper, are usually employed to generate the SPP. However, their refractive index and permittivity cannot be arbitrarily

adjusted. For this reason, the PIT cannot be regulated and cannot meet the needs of dynamic adjustment necessary in several applications. To overcome this issue, researchers gradually turned their attentions to a 2D material, graphene, which is an allotrope of graphite with a thickness of only one atomic layer. Its refractive index and permittivity can be dynamically adjusted by modifying its Fermi energy or voltage [11, 12]. Based on this feature, researchers have proposed and investigated several graphene-based tunable PIT schemes [13-15]. Recently, a material similar to graphene has attracted a large interest in the scientific community. This material is the bulk Dirac semimetal (BDS), also known as the 3D Dirac semimetal. As a three-dimensional analog of graphene, the optical properties of the BDS can also be adjusted via its Fermi energy. However, this material does exhibit a high electron mobility. For example, at the temperature of 5 K, its mobility can reach 9×10^6 cm²/V/s [16], whereas the mobility of graphene measures 2×10^5 cm²/V/s [11]. Several BDS-based SPP and PIT implementation schemes have been proposed and compared with the graphene-based ones [17-22]. Chen et al. designed a metamaterial based on BDS with each unit cell containing an H-shaped structure [17]. The two side strips of the H-shaped structure serve as the dark SPP modes, whereas the central one serves as the bright SPP mode. The interplay between the bright and dark modes is at the basis of the PIT phenomenon. Chen et al. extended this scheme to include two H-shaped structures per unit cell [18]. Differently from Ref. [17], the authors of Ref. [19] used the interplay between two bright modes to achieve the PIT in BDS. The unit cell of such structure consists of two BDS blocks with different sizes. Each block acts as a bright SPP mode. The weak hybridization between them generates the tunable PIT effect in the BDS material. A simpler BDS-based PIT system was proposed and investigated in Ref. [20]. Zhao et al. [21] introduced a BDS-based metamaterial able to achieve a tunable multiple PIT effect. Such metamaterial used a slightly more complex unit cell with four different BDS rods on a dielectric substrate. According to the electric field distributions provided in Ref. [21], the generation

of the multiple PIT effect was originated from the introduction of the bonding mode between the different rods in addition to the bright-bright mode coupling. Wang et al. described a terahertz metamaterial structure [22] with a fourfold symmetry unit cell. They found that the PIT effect being not sensitive to polarization can be achieved by using BDS. Unfortunately, the aforementioned solutions are all based on three-dimensional structures, which are not suitable to develop 2D planar BDS waveguide devices. Recently, Zhai and her collaborators proposed and verified an interesting 2D SPP device based on the BDS material [23]. The basic components of this waveguide device are a side-coupled T-shaped cavity. They found that PIT effect on terahertz band can be achieved in such plasmonic system by introducing a position offset. However, the maximum group delay time that this device can provide is only 11.001 ps.

Due to their different refractive index, many methods developed to achieve PIT in silver or graphene cannot be directly applied to BDS. In this paper, the optical properties of the BDS were investigated and a tunable terahertz plasmonic device generating the PIT effect is proposed. The finite element method (FEM) was carried out in COMSOL Multiphysics to explore the SPP characteristics of the proposed device and reveal the origin of the PIT effect. The basic components of such solution are a BDS waveguide, a rectangular resonator, and a mushroom-shaped resonator. The two resonators are directly coupled to the BDS waveguide, and, for this reason, each resonator can be treated as a bright mode. The interplay between two bright modes lead to the PIT effect in the proposed device. The electrical tunability of the PIT effect was investigated and demonstrated, and the influence of the structural parameters was also considered. The group time delay was calculated to check and measure the subluminal light propagation, i.e., the “slow light” [24]. Furthermore, in order to enhance the PIT effect, multiple cascading devices were designed and their SPP characteristics were investigated. Finally, a refractive index sensor based on the BDS waveguide was developed and its sensing performance was calculated. The results of this work provide a useful reference for the development of novel BDS-based plasmonic devices.

II. STRUCTURE AND MATERIALS

Two main generation mechanisms are known to be at the basis of the PIT effect in metal-insulator-metal (MIM) waveguides. The first one is the bright-dark mode coupling, and the other is the bright-bright mode coupling. In this work, the latter mechanism was chosen to induce the PIT effect in the BDS waveguide. For this purpose, a mushroom-shaped resonator (MSR) and a rectangular resonator (RR) were carefully designed to

provide the bright modes. Their arrangement in the vicinity of the BDS waveguide is shown in Fig. 1. The connection between the BDS waveguide and the resonators is a direct coupling, and both the MSR and the RR serve as the bright modes. The radius and height of the MSR are here labelled as R and h_m , respectively. The width and height of the RR are denoted as W_r and h_r , respectively. The width of the BDS waveguide is W_g . The white area in Fig. 1 represents the air, whereas the dark gray area represents the Dirac semimetal.

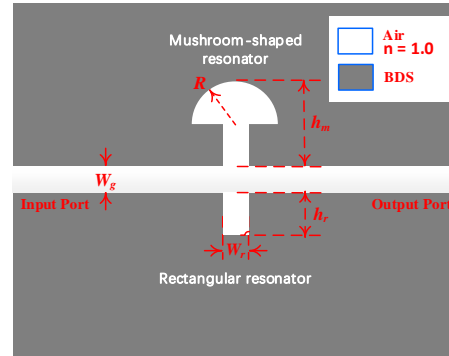


Fig. 1. Schematic diagram of proposed BDS-based plasmonic device.

A three-dimensional Dirac semimetal is an unusual quantum material with massless Dirac fermions. It typically possesses the Fermi - Arc surface states. Common BDS materials include Cd_3As_2 , Na_3Bi , and ZrTe_5 [25]. By only considering the electronic intra-band transition, the permittivity of the 3D Dirac semimetals can be described via a Drude-like formula [16]. This expression is called the one-band model. Alternatively, both the electronic inter-band and intra-band transitions can be taken simultaneously into account. This model is known as the two-band model and it more accurately describes the optical properties of the BDS. Herein, the two-band model was used to derive the expression of the relative permittivity of the BDS material:

$$\varepsilon = \varepsilon_b + j \frac{\sigma}{\omega \varepsilon_0}. \quad (1)$$

Here, σ corresponds to the total dynamic conductivity of the BDS material, ε_0 to the permittivity of vacuum, and ω to angular frequency of the light. Moreover, ε_b is the effective background dielectric constant and its value is set to 1. The tool used to calculate the longitudinal conductivity, σ , was the Kubo-Greenwood formulation in the random-phase approximation (RPA) [26, 27]. From this theory, when the long-wave and low temperature limits are met, the complex conductivity of the sample can be written as follows [28]:

$$\begin{aligned} \text{Re}\sigma(\Omega) &= \frac{e^2}{\hbar} \frac{gk_F}{24\pi} \Omega \theta(\Omega - 2) \\ \text{Im}\sigma(\Omega) &= \frac{e^2}{\hbar} \frac{gk_F}{24\pi^2} \left\{ \frac{4}{\Omega} - \Omega \ln \left(\frac{4\varepsilon_c^2}{|\Omega^2 - 4|} \right) \right\}, \end{aligned} \quad (2)$$

where $g = 40$, e , and \hbar represent the degeneracy factor, the electron charge, and the reduced Planck constant, respectively. The Fermi energy of the BDS material can be written as E_F . In addition, $\varepsilon_c = E_c/E_F$ represents the ratio between the cut-off energy E_c and the Fermi energy E_F . The cut-off energy, E_c , specifies the linear range of the Dirac spectrum. In Eq. (2), the Fermi momentum is defined by $k_F = E_F/\hbar v_F$, where v_F corresponds to the Fermi velocity with a value of 10^6 m/s in this work. In order to take into account the Drude damping, the following expression was used to describe the photon energy $\Omega = \hbar\omega/E_F + j\hbar\tau^{-1}/E_F$. Here, τ represents the carrier relaxation: its expression is $\tau = \mu E_F/ev_F^2$, where the carrier mobility can be defined as $\mu = 3 \times 10^4$ cm²/V/s. Figure 2 displays the real and the imaginary parts of the dynamic conductivity of the BDS material at different Fermi energies.

III. RESULTS AND DISCUSSION

To clarify the physics behind the PIT effect generation, the transmission spectrum and the mode field distributions for the device shown in Fig. 1 were calculated. The finite element method provided by the commercial software COMSOL Multiphysics was used for this purpose. The scattered waves, escaping the computational region, are absorbed by the perfectly matched layer (PML) boundary condition. The transmittance (T) and the reflectivity (R) were calculated according to the following expressions:

$$T = |S_{21}|^2 \quad R = |S_{11}|^2, \quad (3)$$

here, S_{21} and S_{11} are the scattering matrix elements of the device. The optical absorption of the device was determined via the formula $A = 1 - R - T$. The results for an energy $E_F = 75$ meV with optimized structural parameters $W_g = W_r = 50$ μm , $R = 200$ μm , $h_m = 280$ μm , and $h_r = 80$ μm , are shown in Fig. 3. The transmission spectrum is represented by a red solid line in Fig. 3, whereas the reflection spectrum is shown by the blue dashed line. The distributions of the magnetic field, H_z , for the 320.4 μm , 347.2 μm , and 361 μm wavelengths are shown in the insets of Fig. 3. The results show that a transmission peak, also known as the transparency window, with its central wavelength at 347.2 μm appears

in the transmission spectrum. The occurrence of the PIT effect in the device can be attributed to the coupling between the detuned resonators. The MSR and RR can be treated as two detuned resonators, which provide different light paths for the incident waves. When the optical signals from the different optical paths couple back into the output waveguide, the coherent interference between them results in the generation of the PIT effect. In order to investigate the subluminal propagation of the light caused by the PIT the transmitted phase, $\phi(\omega)$, and the group delay time, t_g , were calculated for the proposed device. The value of t_g was defined by using the first-order derivative of the transmitted phase, $\phi(\omega)$, with respect to the circular frequency, ω . The results are shown in Fig. 4: A group delay-time up to 18.64 ps can be measured for the central wavelength of the PIT window. This observation fully demonstrates that the proposed device exhibits an excellent slow light transmission performance when the PIT effect takes place.

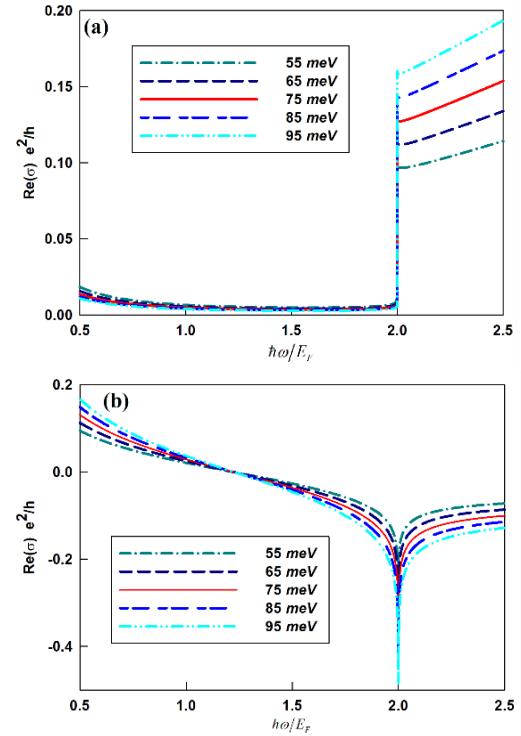


Fig. 2. Real (a) and the imaginary (b) parts of the dynamic conductivity of the BDS material at different Fermi energies. The unit of the vertical axis is e^2/\hbar , while the horizontal axis is the normalized frequency $\hbar\omega/E_F$, $\varepsilon_c = 3$.

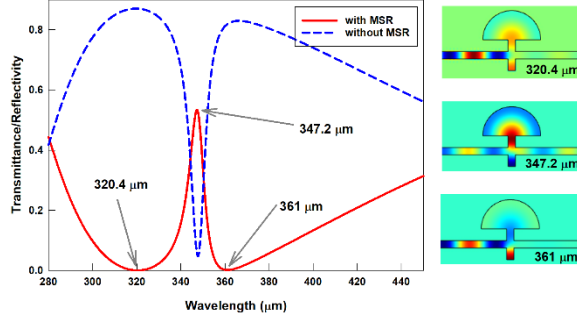


Fig. 3. Transmission and reflection spectra of the proposed device, the insets show the field distribution of H_z at the wavelength of 320.4 μm , 347.2 μm and 361 μm , respectively.

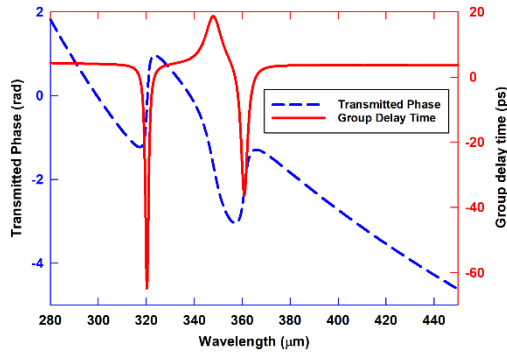


Fig. 4. Variations of the transmitted phase and the group delay time with respect to the wavelength of incident light.

The radius of the semicircular resonant cavity has a large influence on the generation of the PIT effect. To examine its influence, both the transmittance and the group time delay were calculated for the different values of the radius of the MSR. The results are shown in Fig. 5. The variation of the transmission performance of the device with radius R is very remarkable. As R increases, the central wave-length of the PIT window gradually increases, however the maximum transmittance gradually decreases. The variation of the group delay-time as a function of the radius R is shown in Fig. 5 (b). The maximum group delay time at the PIT window also increases upon an increase in the radius R .

Although a variation in the structural parameters can be used to effectively modulate the PIT effect, as shown above, the PIT effect cannot be dynamically adjusted in the range required in many practical applications. However, this can be achieved by adjusting the Fermi energy or the voltage applied to the device. The voltage applied to the device can change the carrier density and Fermi energy of the BDS. Therefore, the PIT effect of the proposed device can also be dynamically controlled

by the voltage. The regulation relationship between Fermi energy E_F and gate voltage V can be explained by a parallel-plate capacitor model [29]. An approximate expression is shown as follows:

$$E_F \approx \hbar v_F \left(\frac{\pi \epsilon_0 \epsilon_d V}{ed} \right)^{1/2}. \quad (4)$$

Here d is the length between the two electrodes, ϵ_d is the relative permittivity of dielectric filled between the two electrodes, and ϵ_0 is the vacuum permittivity. To investigate the effectiveness of this method, the Fermi energy was modified from 55 meV to 95 meV in steps of 10 meV. At each energy step, the transmission spectrum and the group delay time were measured, as shown in Fig. 6. The results in Fig. 6 (a) show that the central wavelength of the PIT window exhibits only a slight redshift as the Fermi energy gradually increases. However, the maximum transmittance at the PIT window, increases upon an increase in the Fermi energy. Increasing the Fermi energy of the BDS increases, in fact, the carrier concentration of the material, and ultimately reduced its losses. Figure 6 (b) shows that by varying the Fermi energy of the BDS the group delay time can be regulated. The maximum group delay time at the PIT window increases with an increase in the Fermi energy, E_F . When $E_F=95$ meV, the maximum group delay time reaches 21 ps.

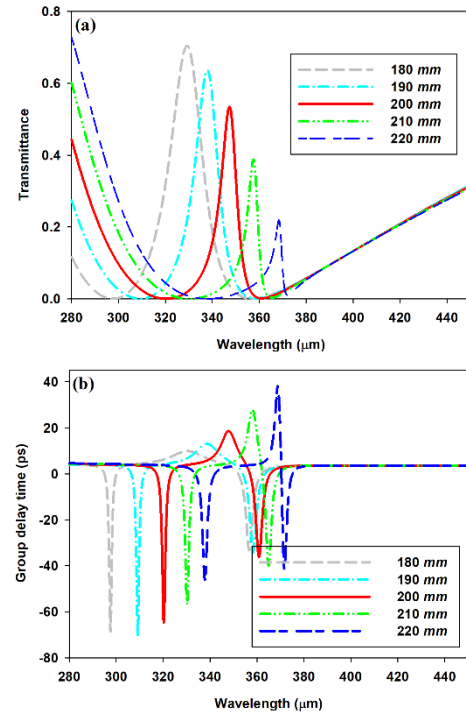


Fig. 5. Transmission spectra (a) and the group delay times (b) of the proposed device for different radius.

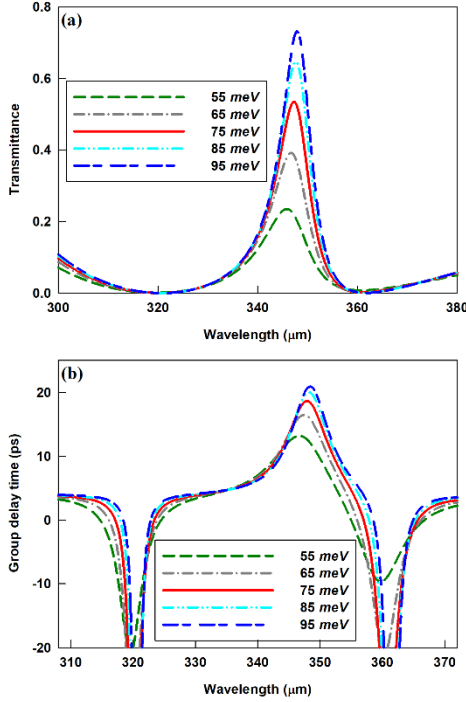


Fig. 6. Transmission spectra (a) and the group delay times (b) of the proposed device for different Fermi energy.

An important application of the PIT effect is the manufacturing of refractive index sensors. The BDS-based plasmonic device proposed in this work can as well be used as a refractive index sensor. In this scenario, the refractive index of the environment varies with the analyte to be monitored, such as a contaminated gas. To investigate the refractive index sensitivity of such device, the ambient refractive index was varied in the 1–1.06 range with a step of 0.01. The transmission spectrum of the device at each ambient refractive index is shown in Fig. 7. As the ambient refractive index increases, the central wavelength of the PIT window increases as well, exhibiting a redshift. The refractive index sensitivity is defined as $S = \Delta f / \Delta n$, where Δf corresponds to the central frequency shift of PIT window, Δn to the variation in the ambient refractive index. According to Fig. 7, the average frequency shift of the center of the PIT window is 0.00821 THz per 0.01 increment in the ambient refractive index value. This measurement provides a refractive index sensitivity of 0.821 THz per RIU.

In order to further enhance the PIT effect, a cascading device with configuration shown in Fig. 8 (a) was designed. This device contains two meta-atoms, each consisting of a mushroom-shaped resonator and a rectangular resonator. The spatial separation between them

is $S = 250 \mu\text{m}$. The values of R , h_r , and h_m were fixed to 200, 80, and 280 μm , respectively. The Fermi energy measured $E_F = 75 \text{ meV}$. The calculated transmittance and the group delay time for this cascading device are shown in Fig. 8 (b): The maximum transmittance of the PIT window appears to be significantly reduced when compared to the non-cascading device. The optical impulse is scattered and then, absorbed when it passes through each meta-atom. Therefore, upon an increase in the meta-atom concentration, a higher energy loss takes place. Nevertheless, the group delay time, t_g , is greatly enhanced in the cascading device. As shown in the inset of Fig. 8 (b), t_g at the central wavelength of the PIT window increases from 18.64 ps to 37.78 ps.

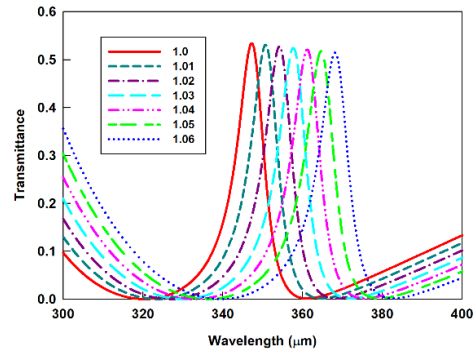


Fig. 7. Transmission spectra of the proposed device for different refractive indices of the analytes.

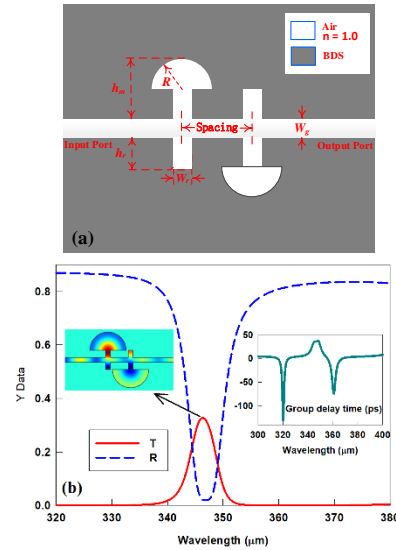


Fig. 8. Schematic diagram (a) and transmission performance (b) of the cascading device, the insets of (b) show the group delay time and the distribution of the magnetic field.

The performance of the electrically tunable PIT of the cascading device is shown in Fig. 9. The transmittance and the group delay time were measured at different Fermi energies and the results are shown in Figs. 9 (a) and (b), respectively. Figure 9 (a) shows that the maximum transmittance at the PIT window increases as a function of E_F . When E_F reaches 95 meV, the maximum transmittance can even approach 0.6. This indicates that increasing the Fermi energy is an effective means to compensate for the transmission losses present in the cascading device. The group delay time can similarly be enhanced by modulating the Fermi energy. Figure 9 (b) shows that as the Fermi energy increases from 55 meV to 95 meV, the maximum group delay time at the PIT window increases to 44.57 ps.

Finally, the impact of the ambient refractive index on the PIT effect of the cascading device was investigated. To perform this series of measurements, the ambient refractive index was increased from 1.0 to 1.06 in steps of 0.01. The transmittance of the cascading device as a function of the ambient refractive index is shown in Fig. 10. As in the case of the non-cascading device, the center frequency of the PIT window of the cascading one exhibits a redshift with an increase in the ambient refractive index. At each 0.01 increment, the average shift of the central frequency of the PIT window measures 0.0082 THz. This indicates that the cascading device has a sensitivity of 0.82 THz per RIU.

As we can see from Figs. 7-10, the more meta-atoms are cascaded, the larger propagation loss conspicuously becomes. The propagation loss is the obstacle that hinders the practical application of the cascade scheme. One possible solution is to replace the passive dielectric part of the cascade device with gain material [30] or nonlinear material [31] to compensate for propagation loss. In Table 1, the slow-light performance of different designs is compared with that of our proposed device. One can see that our proposed device is capable of providing a group delay time of up to 44.57 ps if two meta-atoms are used in cascade. The device in [35] also exhibits very high group delay time. However, the device is a three-dimensional structure and cannot be two-dimensionally integrated in a chip. Our results fully demonstrate the advantages of the BDS-based plasmonic device in terms of slow light performance.

In the end, it is valuable to discuss the experimental implementability of the device proposed in this paper. So far, three preparation methods of BDS films have been proposed, which are melt growth [36], chemical vapor deposition [37] and molecular beam epitaxy [38]. After the BDS film is fabricated, the waveguide and resonant cavity shown in Fig. 1 can be prepared experimentally using photoresist technology and dry etching [39]. Thus, the solution proposed in this paper is fully implementable on experiments.

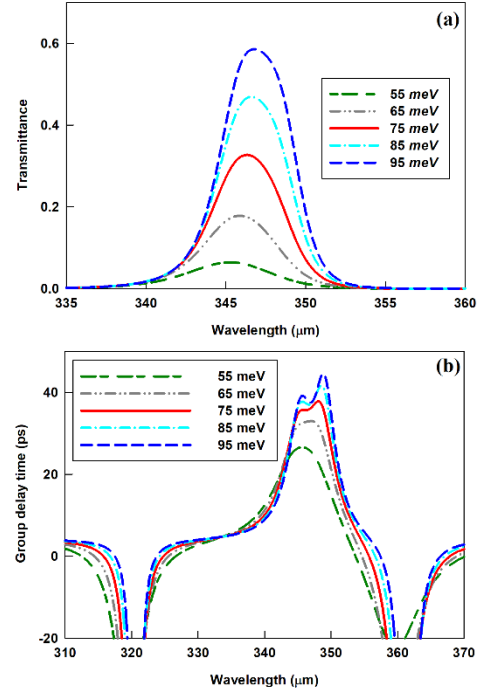


Fig. 9. Transmission spectra (a) and the group delay times (b) of the cascading device for different E_F .

Table 1: Comparison of the proposed device and other published designs

Reference	Dimension	Material	Group Delay Time (ps)
[32]	2D	Silver	1.8
[33]	2D	Graphene	1.1
[34]	3D	Graphene	13.28
[35]	3D	Graphene	43
[17]	3D	BDS	6.81
[23]	2D	BDS	11.001
This work	2D	BDS	44.57

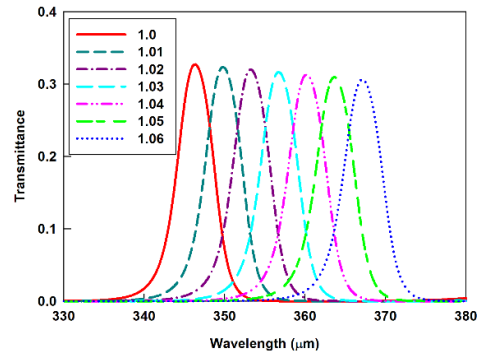


Fig. 10. Transmission spectra of the cascading device for different refractive indices of the analytes.

VI. CONCLUSION

In summary, a solution to generate the PIT effect in BDS materials was proposed and investigated. Initially, the origin of the PIT effect was discussed and explained based on the transmission spectra and the field distributions. Then, the electrical tunability and the influence of the structural parameters were investigated in detail. According to the results, a group delay time up to 44.57 ps can be achieved with the proposed plasmonic device. If the ambient refractive index changes, the central wavelength of the PIT window of the device shifts remarkably. These observations suggest that the solution proposed in this work can provide a useful reference for the production of both high-performance slow-light devices and refractive index sensors.

ACKNOWLEDGMENT

This work was supported in part by the National Natural Science Foundation of China (no. 61367007); the Natural Science Fund of Gansu Province of China (no. 20JR10RA154).

REFERENCES

- [1] X. X. Niu, X. Y. Hu, Q. C. Yan, J. K. Zhu, H. T. Cheng, Y. F. Huang, C. C. Lu, Y. L. Fu, and Q. H. Gong, "Plasmon-induced transparency effect for ultracompact on-chip devices," *Nanophotonics*, vol. 8, no. 7, pp. 1125-1149, July 2019.
- [2] A. M. Akulshin, S. Barreiro, and A. Lezama, "Steep anomalous dispersion in coherently prepared Rb vapor," *Physical Review Letters*, vol. 83, no. 21, pp. 4277-4280, 1999.
- [3] H. Failache, P. Valente, G. Ban, V. Lorent, and A. Lezama, "Inhibition of electromagnetically induced absorption due to excited-state decoherence in Rb vapor," *Physical Review A*, vol. 67, no. 4, p. 043810, 2003.
- [4] M. F. Yanik, W. Suh, Z. Wang, and S. H. Fan, "Stopping light in a waveguide with an all-optical analog of electro-magnetically induced transparency," *Physical Review Letters*, vol. 93, no. 23, p. 233903, 2004.
- [5] N. Papasimakis, V. A. Fedotov, N. I. Zheludev, and S. L. Prosvirnin, "Metamaterial analog of electromagnetically induced transparency," *Physical Review Letters*, vol. 101, no. 25, p. 253903, 2008.
- [6] F. M. Liu, M. Z. Ke, A. Q. Zhang, W. J. Wen, J. Shi, Z. Y. Liu, and P. Sheng, "Acoustic analog of electromagnetically induced transparency in periodic arrays of square rods," *Physical Review E*, vol. 82, no. 2, p. 026601, Aug. 2010.
- [7] Y. Yang, I. I. Kravchenko, D. P. Briggs, and J. Valentine, "All-dielectric metasurface analogue of electromagnetically induced transparency," *Nature Communications*, vol. 5, no. 1, pp. 1-7, Dec. 2014.
- [8] Z. R. Zhang, L. W. Zhang, H. Q. Li, and H. Chen, "Plasmon induced transparency in a surface plasmon polariton waveguide with a comb line slot and rectangle cavity," *Applied Physics Letters*, vol. 104, no. 23, p. 231114, June 2014.
- [9] Z. H. He, H. J. Li, S. P. Zhan, G. T. Cao, and B. X. Li, "Combined theoretical analysis for plasmon-induced transparency in waveguide systems," *Optics Letters*, vol. 39, no. 19, pp. 5543-5546, Oct. 2014.
- [10] J. J. Chen, Z. Li, S. Yue, J. J. Xiao, and Q. H. Gong, "Plasmon-induced transparency in asymmetric T-shape single slit," *Nano Letters*, vol. 12, no. 5, pp. 2494-2498, Apr. 2012.
- [11] G. X. Ni, A. S. McLeod, Z. Sun, L. Wang, L. Xiong, K. W. Post, S. S. Sunku, B. Y. Jiang, J. Hone, C. R. Dean, M. M. Fogler, and D. N. Basov, "Fundamental limits to graphene plasmonics," *Nature*, vol. 557, no. 7706, pp. 530-533, May 2018.
- [12] Y. C. Fan, N. H. Shen, F. L. Zhang, Q. Zhao, H. J. Wu, Q. H. Fu, Z. Y. Wei, H. Q. Li, and C. M. Soukoulis, "Graphene plasmonics: A platform for 2D optics," *Advanced Optical Materials*, vol. 7, no. 3, p. 1800537, Dec. 2018.
- [13] X. L. Zhao, C. Yuan, L. Zhu, and J. Q. Yao, "Graphene-based tunable terahertz plasmon-induced transparency metamaterial," *Nanoscale*, vol. 8, no. 33, pp. 15273-15280, July 2016.
- [14] H. Xu, M. Z. Zhao, M. F. Zheng, C. X. Xiong, B. H. Zhang, Y. Y. Peng, and H. J. Li, "Dual plasmon-induced transparency and slow light effect in monolayer graphene structure with rectangular defects," *Journal of Physics D: Applied Physics*, vol. 52, no. 2, p. 025104, Nov. 2018.
- [15] X. Y. He, F. Liu, F. T. Lin, and W. Z. Shi, "Graphene patterns supported terahertz tunable plasmon induced transparency," *Optics Express*, vol. 26, no. 8, pp. 9931-9944, Apr. 2018.
- [16] O. V. Kotov, and Y. E. Lozovik, "Dielectric response and novel electromagnetic modes in three-dimensional Dirac semimetal films," *Physical Review B*, vol. 93, no. 23, p. 235417, June 2016.
- [17] H. Chen, H. Y. Zhang, X. H. Guo, S. D. Liu, and Y. P. Zhang, "Tunable plasmon-induced transparency in H-shaped Dirac semimetal metamaterial," *Applied Optics*, vol. 57, no. 4, pp. 752-756, Feb. 2018.
- [18] H. Chen, H. Y. Zhang, M. D. Liu, Y. K. Zhao, S. D. Liu, and Y. P. Zhang, "Tunable multiple plasmon-induced transparency in three-dimensional Dirac semimetal metamaterials," *Optics Communications*, vol. 423, pp. 57-62, Sep. 2018.
- [19] S. Yang, R. L. Zhou, D. Liu, Q. W. Lin, and S. Li, "Controlling the plasmon-induced transparency system based on Dirac semimetal at mid-infrared

- band,” *Optics Communications*, vol. 449, pp. 13-18, Oct. 2019.
- [20] H. Chen, H. Y. Zhang, M. D. Liu, Y. K. Zhao, X. H. Guo, and Y. P. Zhang, “Realization of tunable plasmon-induced transparency by bright-bright mode coupling in Dirac semimetals,” *Optical Materials Express*, vol. 7, no. 9, pp. 3397-3407, Sep. 2017.
- [21] J. X. Zhao, J. L. Song, Y. Zhou, R. L. Zhao, and J. H. Zhou, “Tunable multiple plasmon-induced transparency in a simple terahertz Dirac semi-metal based metamaterial,” *Optical Materials Express*, vol. 9, no. 8, pp. 3325-3332, Aug. 2019.
- [22] T. L. Wang, M. Y. Cao, Y. P. Zhang, and H. Y. Zhang, “Tunable polarization-nonsensitive electromagnetically induced transparency in Dirac semimetal metamaterial at terahertz frequencies,” *Optical Materials Express*, vol. 9, no. 4, pp. 1562-1576, Apr. 2019.
- [23] T. Zhou, X. Y. Gou, W. Xu, Y. Li, X. Zhai, H. Li, and L. Wang, “Dynamically tunable plasmon-induced transparency in a T-shaped cavity waveguide based on bulk Dirac semimetals,” *Plasmonics*, vol. 16, no. 2, pp. 323-332, 2021.
- [24] D. Bortman-Arbiv, A. D. Wilson-Gordon, and H. Friedmann, “Phase control of group velocity: From subluminal to superluminal light propagation,” *Physical Review A*, vol. 63, no. 4, p. 043818, 2001.
- [25] T. Liang, Q. Gibson, M. N. Ali, M. H. Liu, R. J. Cava, and N. P. Ong, “Ultrahigh mobility and giant magnetoresistance in the Dirac semimetal Cd_3As_2 ,” *Nature Materials*, vol. 14, no. 3, pp. 280-284, Mar. 2015.
- [26] V. P. Gusynin, S. G. Sharapov, and J. P. Carbotte, “Magneto-optical conductivity in graphene,” *Journal of Physics: Condensed Matter*, vol. 19, no. 2, p. 026222, Dec. 2006.
- [27] G. W. Hanson, “Dyadic Green’s functions and guided surface waves for a surface conductivity model of graphene,” *Journal of Applied Physics*, vol. 103, no. 6, p. 064302, Mar. 2008.
- [28] H. Xiong, Q. Shen, and Q. Ji, “Broadband dynamically tunable terahertz absorber based on a Dirac semimetal,” *Applied Optics*, vol. 59, no. 16, pp. 4970-4976, May 2020.
- [29] J. S. Gómez-Díaz and J. Perruisseau-Carrier, “Graphene-based plasmonic switches at near infrared frequencies,” *Optics Express*, vol. 21, no. 13, pp. 15490-15504, June 2013.
- [30] N. Liu, H. Wei, J. Li, Z. X. Wang, X. R. Tian, A. L. Pan, and H. Xu, “Plasmonic amplification with ultra-high optical gain at room temperature,” *Scientific Reports*, vol. 3, p. 1967, June 2013.
- [31] B. Liu, Y. C. Liao, J. F. Hu, J. Liu, X. D. He, and Z. P. Chen, “Plasmon-induced reflection and its application for all-optical diode based on paralleled double-stub resonators,” *Applied Physics Express*, vol. 12, no. 3, p. 032011, Feb. 2019.
- [32] Y. J. Zhu, T. Wang, X. Han, and B. Y. Wang, “Plasmon-induced transparency effect in a single circular split-ring core ring resonator side-coupled to a metal-isolator-metal waveguide,” *Journal of Applied Physics*, vol. 117, no. 13, p. 133108, Apr. 2015.
- [33] P. Qiu, W. Qiu, Z. Lin, H. B. Chen, J. B. Ren, J. X. Wang, Q. Kan, and J. Q. Pan, “Dynamically tunable plasmon-induced transparency in on-chip graphene-based asymmetrical nanocavity-coupled waveguide system,” *Nanoscale Research Letters*, vol. 12, no. 1, pp. 1-8, May 2017.
- [34] W. Jia, P. Ren, Y. Jia, and C. Fan, “Active control and large group delay in graphene-based terahertz metamaterials,” *Journal of Physical Chemistry C*, vol. 123, no. 30, pp. 18560-18564, July 2019.
- [35] X. Yan, T. Wang, S. Xiao, T. Liu, H. Hou, L. Cheng, and X. Jiang, “Dynamically controllable plasmon induced transparency based on hybrid metal-graphene metamaterials,” *Scientific Reports*, vol. 7, no. 1, pp. 1-10, Oct. 2017.
- [36] M. N. Ali, Q. Gibson, S. Jeon, B. Zhou, A. Yazdani, and R. J. Cava, “The crystal and electronic structures of Cd_3As_2 , the three-dimensional electronic analogue of graphene,” *Inorganic Chemistry*, vol. 53, no. 8, pp. 4062-4067, 2014.
- [37] A. Wang, P. Xiang, X. Ye, W. Zheng, D. Yu, and Z. Liao, “Surface engineering of antisymmetric linear magnetoresistance and spin-polarized surface state transport in Dirac semimetals,” *Nano Letters*, vol. 21, no. 5, pp. 2026-2032, 2021.
- [38] Y. Nakazawa, M. Uchida, S. Nishihaya, S. Sato, A. Nakao, J. Matsuno, and M. Kawasaki, “Molecular beam epitaxy of three-dimensionally thick Dirac semimetal Cd_3As_2 films,” *APL Materials*, vol. 7, no. 7, p. 071109, 2019.
- [39] W. Nickel, M. Oschatz, S. Rico-Francés, S. Klosz, T. Biemelt, G. Mondin, A. Eychmüller, J. Silvestre-Albero, and S. Kaskel, “Synthesis of ordered mesoporous carbon materials by dry etching,” *Chemistry*, vol. 21, no. 42, pp. 14753-14757, 2015.



Daobin Wang was born in 1976. He received the B.S. degree from Xi’an Jiaotong University and the Ph.D. degree from Beijing University of Posts and Telecommunication, Beijing, China. He is currently an Associate Professor at Lanzhou University of Technology, Lanzhou, China. His research interests include optical fiber communication, radio over fiber, and nano-photonics.